Integrated Bidirectional Three-Port DC–DC Converter with Ripple-Free Input Current and Soft Switching

Parastou KhademiAstaneh[*], Javad Javidan[†], Khalil Valipour[*], and Adel Akbarimajd[*]

[†,*]Technical Engineering Department, University of Mohaghegh Ardabili, Ardabil, Iran

Abstract

Multiport power converters have recently become popular to researchers and engineers. However, more improvements are required in terms of their soft-switching operation, bidirectional operation, and integration. In this study, a bidirectional three-port three-switch DC–DC converter is proposed. The converter contains a low-current ripple port and ripple-free current port. Through the integrated structure, utilization of a coupled inductor, and a new switching strategy, the aforementioned specifications are achieved. A modified switching strategy is also utilized in the converter, which has resulted in the bidirectional operation of the converter between ports. Finally, a comprehensive analysis is presented, and the converter characteristics are validated by experimental results.

Key words: Bidirectional port, Multiport DC–DC converter, Renewable energy, Ripple-free port, Soft switching

I. INTRODUCTION

The increase in air pollution and global warming and the reduction of fossil fuel resources have urged engineers to use green energies, such as wind and photovoltaic energies. The use of power electronics has been essentially applicable for utilizing these types of energy resources [1]-[4]. However, due to the reliability problems of such resources, utilizing energy storage units and other energy resources aside from the main energy resource is inevitable [5]-[10]. These systems can consist one unique converter having several ports, and all energy resources and loads are connected to the converter. The aforementioned unique converter is called multi-input or multiport converter. Utilizing such converters has the advantages of increasing system efficiency and reliability and improving system dynamics due to the use of a central controller.

Many converters have been proposed in the literature to manage power between different sources. Refs. [11]-[14]

discussed multiport converters with time-sharing strategy to control power. In such converters, a complex control strategy is required, which is the result of changing the switching pattern in various power transfer situations. In Ref. [15], a family of three-port converters was introduced by integrating conventional buck, boost, and buck boost converters. In Ref. [16], an isolated double-input DC–DC converter was proposed based on the use of an alternative pulsating source. In Ref. [17], a four-port DC–DC converter with soft-switching and time-sharing power management strategy was introduced. In Ref. [18], a four-port converter was proposed based on transformer isolation. However, the aforementioned converters suffer from bidirectional operation and soft-switching performance. To achieve bidirectional operation, Ref. [19] proposed a novel structure, which however suffers from the hard switching operation of the switches. In addition, the converter utilizes six semiconductors, which increases cost. In Ref. [20], a single-inductor three-port converter was proposed in which a special structure called storage-switch diode is used. The aforementioned converter includes bidirectional operation, but it utilizes six semiconductor components and the input ports suffer from current ripples. The aim of this study is to propose a converter with a low number of semiconductor components and low current ripple.

Current ripples can affect the efficiency of power sources especially for fuel cells.

In this study, a three-port DC–DC converter was proposed based on the topology presented in Ref. [6]. The proposed structure utilizes three switches with a special switching strategy, which enables the converter to transfer power from one port to another and allows the converter to always operate in a continuous conduction mode. In addition, through the utilization of a coupled inductor in the topology, the current of port 2 became ripple free, which is excellent for renewable energy resources as their performance depends on the current ripple. The main features of the proposed converter are listed below:

- Utilization of only three switches
- Bidirectional operation of all ports
- Simple controller is required due to single-mode operation (only one switching modulation is used for all power flow directions).
- Soft switching of three switches
- Ripple-free input current of port 2

The paper is organized as follows. Section II reviews the conventional three-switch converter and presents the operating modes of such converter. Section III presents the proposed improved structure, whose main capabilities are soft switching, ripple-free input current, and bidirectional operation of all ports. In this section, the operation of proposed converter is also presented for all time intervals. Section IV comprehensively discusses design considerations. Finally, Section V illustrates the experimental results that validate the performance of the proposed converter.

II. CONVENTIONAL THREE-SWITCH CONVERTER

The three-switch converter proposed in Ref. [6] is illustrated in Fig. 1(a). The converter, which contains three switches, two inductors, and one capacitor, operates as an integrated boost–boost converter. The switching pattern applied to the converter is shown in Fig. 1(b), in which S_1 and S_2 are triggered complementarily. As shown in the figure, the converter includes five time intervals. To investigate the converter operation, the following initial conditions of the converter (the status of the converter at time $t=t_0^-$) are considered:

- $i_1(t_0^-) = I_1^{min}$, $i_2(t_0^-) = I_2^{max}$.
- All the parasitic components of the circuit are neglected.

Consequently, the operating intervals can be described as follows:

Interval 1—[t_0, t_1]: At time $t=t_0$, S_2 is turned off. After that, if $I_2^{max} > 0$, then a soft switching of switch S_1 may occur. That is, if $I_2^{max} > 0$, by turning off switch S_2, then current i_2 will flow through the drain-source capacitors of S_1 and S_2.
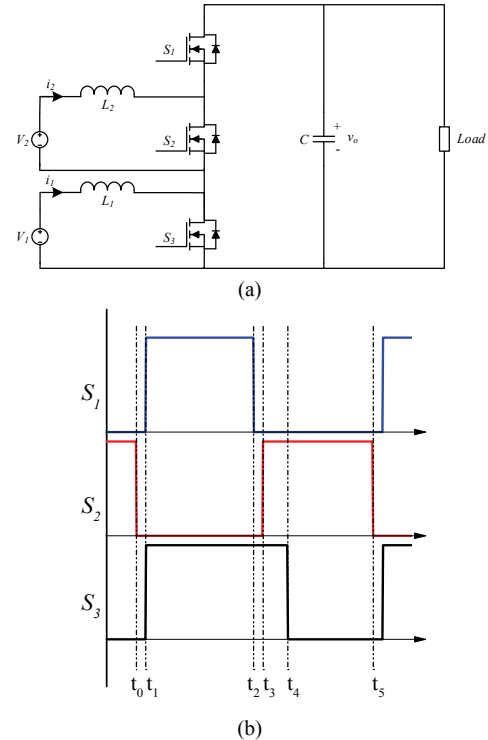

(a)

(b)

Fig. 1. Conventional three-switch converter: (a) Circuit, (b) Gates' pulses.

This event results in the discharging of C_{DS,S_1} and the charging of C_{DS,S_2}.

After C_{DS,S_1} discharges, the current flows through the body diode of S_1. Hence, V_{DS,S_2} becomes turned on in a zero voltage switching (ZVS) condition.

Interval 2—[t_1, t_2]: At the start of this interval, S_3 is turned on. Consequently, L_1 starts to store energy while L_2 releases its energy to output capacitor C.

Interval 3—[t_2, t_3]: In this interval, S_1 is turned off. Hence, if its current is larger than zero, then switch S_2 may be turned on in a soft-switching condition.

Interval 4—[t_3, t_4]: During this interval, switches S_2 and S_3 are turned on. Consequently, L_1 and L_2 are charged and the output port is supplied by the output capacitor. At the end of this interval, S_3 is turned off.

Interval 5—[t_4, t_5]: In this interval, only switch S_2 is turned on. Then, L_1 is charged and L_2 releases its energy into the output capacitor.

According to the time-interval description, the conventional converter will operate in a soft-switching condition only if port 2, which is presented in Fig. 1a, supplies the power and its ripple is higher than the average of its current. In addition, as shown in Fig. 1b, when S_3 is turned off, S_1 is also turned off. Therefore, in the point of view of port 1, the converter operates similarly to a unidirectional boost converter.

In the next section, a modified converter is proposed using new switching strategies, which lead to bidirectional operation

of all ports and result in a soft-switching condition of all switches.

III. PROPOSED THREE-SWITCH CONVERTER

The proposed converter is shown in Fig. 2 in details. In this structure, inductance L_2 is replaced by a coupled inductor. The coupled inductor enable port 2 to have ripple-free current, which then leads the switches to operate in soft-switching conditions. In addition, the proposed switching pattern, which is shown in Fig. 3, results in the bidirectional operation of the converter. To analyze the converter, it is assumed that it operates in a steady-state condition and switches S_1 and S_2 are turned on before time $t=t_0$. Consequently, magnetizing the inductance of L_2 and L_m is charged by input source V_2. Indeed, the energy of L_1 charges output capacitor C. The following assumptions are considered for the starting time of the analysis:

- $i_1(t_0) = I_1^{min}$, $i_m(t_0) = I_m^{max}$, $i_k(t_0) = I_k^{max}$.
- The coupled inductor is modeled as an ideal transformer with a magnetizing inductance in parallel with the primary side and a series leakage inductance in the secondary side.
- All parasitic components are neglected, except the parasitic capacitor of the switches, which is used for the discussions on soft switching.

Consequently, the operating intervals shown in Fig. 4 can be described as follows:

Interval 1—[t_0, t_1]: At the start of this interval, S_2 is turned off [Fig. 4(a)]. Therefore, i_2, which flew through S_2, starts to flow through the drain-source capacitors of S_3 and S_2. Accordingly, $C_{DS\,S_2}$ is charged, and simultaneously, $C_{DS\,S_3}$ is discharged. Subsequently, the current starts to flow through the body diode of S_3. By flowing the current through it, $V_{DS\,S_3}$ remains zero and S_3 is ready to be turned on in a ZVS condition.

Interval 2—[t_1, t_2]: In this interval, initially, S_3 is turned on in a ZVS condition [Fig. 4(b)]. During this interval, L_1 is charged and currents i_m and i_k start to decrease. Therefore, in this time interval, output capacitance C is charged by the stored energy in L_m and supplies the output load simultaneously. Moreover, in this mode, capacitor C_k is discharged and i_k starts to decrease. Given that C_k is placed in series with L_k, i_k only contains an AC term. Moreover, the current depends on the status of S_2 and reaches its minimum value at the end of the interval. At the start of this interval, i_k is at the maximum positive value, which helps S_3 to be turned on in a ZVS condition. At the end of this interval, i_k reaches the maximum negative value, which leads switch S_2 to be turned on in a ZVS condition in the next intervals. At the end of this interval, switch S_1 is turned off. The mathematical model of this interval can be formulated as follows:

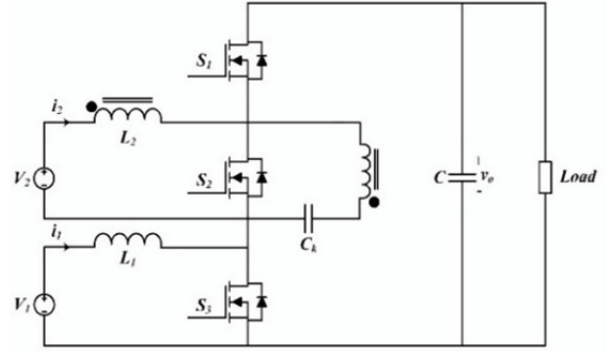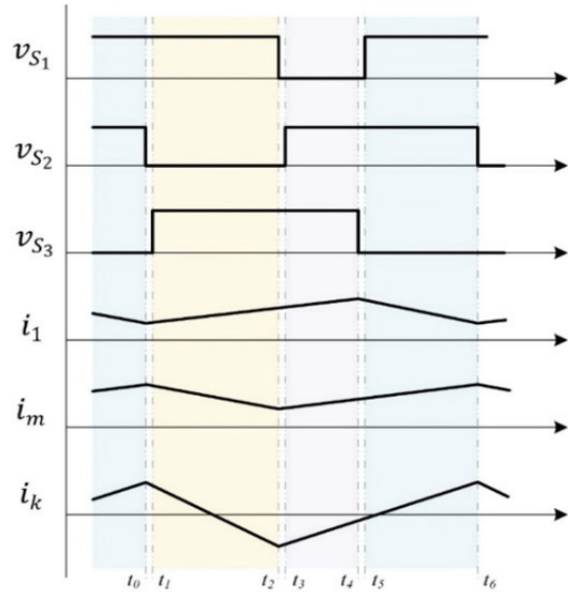Fig. 2. Proposed circuit.

Fig. 3. Key waveforms of the proposed converter.

$$L_1 \frac{di_1}{dt} = v_1 \rightarrow i_1(t) = I_1^{min} + \frac{v_1}{L_1}(t - t_1) . \tag{1}$$

$$L_m \frac{di_m}{dt} = -v_o + v_2 \rightarrow i_m(t) = I_m^{max} + \frac{-v_o + v_1}{L_m}(t - t_1) . \tag{2}$$

$$L_k \frac{di_k}{dt} = v_k - v_o - n(v_2 - v_o) \rightarrow i_k(t) = I_k^{max} + \tag{3}$$

$$\frac{-v_o + v_k - n(v_2 - v_o)}{L_k}(t - t_1)$$

Interval 3—[t_2, t_3]: When S_1 is turned off, its current, which is a positive value (the summation $i_2 + i_k$), will flow through switch S_2 [Fig. 4(c)]. Accordingly, in this interval, the current charges the drain-source capacitor of S_1 and discharges the drain-source capacitor of S_2. The discharging of $C_{DS\,S_2}$ enables the body diode of S_2 to start conducting. Consequently, $V_{DS\,S_2}$ becomes zero.

Interval 4—[t_3, t_4]: At the start of this interval, at time t_3, S_2 is turned on in a ZVS condition, as its voltage became zero in the last interval [Fig. 4(d)]. When switch S_2 is turned on, L_1 and L_m start to store energy. In addition, the secondary voltage of
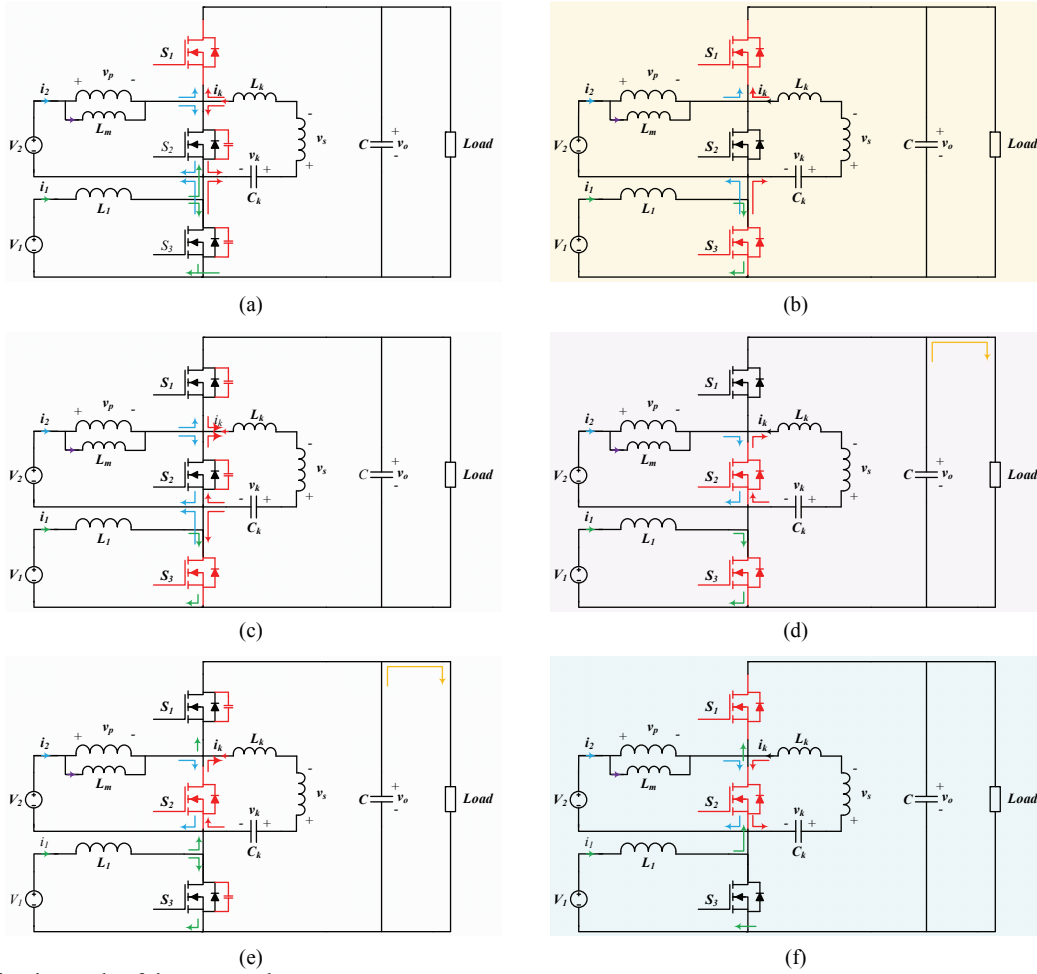
Fig. 4. Operating intervals of the proposed converter.

the coupled inductor charges capacitor C_k. Hence, i_k starts to increase from the minimum voltage to the maximum positive value. Given that switch S_1 is turned off and the other switches are turned on, C discharges to supply the load. At the end of this interval, S_3 is turned off. The mathematical equations describing this interval are as follows:

$$L_1 \frac{di_1}{dt} = v_1 \rightarrow i_1(t) = I_1^{min} + \frac{v_1}{L_1}(t-t_1) , \tag{4}$$

$$L_m \frac{di_m}{dt} = v_2 \rightarrow i_m(t) = -I_m^{min} + \frac{v_2}{L_m}(t-t_3) , \tag{5}$$

$$L_k \frac{di_k}{dt} = v_k - nv_2 \rightarrow i_k(t) = -I_k^{min} + \frac{v_k - nv_2}{L_k}(t-t_3) . \tag{6}$$

Interval 5—[t_4, t_5]: When S_3 is turned off at the start of this interval, i_1 flows through S_3 [Fig. 4(e)]. Then, C_{DS,S_3} is charged and C_{DS,S_1} is discharged. Then, when C_{DS,S_1} is discharged, current i_1 flows through the body diode of S_1. In addition, this current flows through S_2, which leads to the reduction of i_{S_2}. Accordingly, this interval provides S_1 for soft-switching operation.

Interval 6—[t_5, t_6]: At the start of this interval, S_1 is turned

on in a ZVS condition. During this interval, L_m is charged while L_1 sends its stored energy to the output capacitor [Fig. 4(f)]. Given that switch S_2 is turned on, C_k is charged and i_k increases. The mathematical model related to this interval can be expressed as follows:

$$L_1 \frac{di_1}{dt} = v_1 - v_o \rightarrow i_1(t) = I_1^{max} + \frac{v_1 - v_o}{L_1}(t-t_5) , \tag{7}$$

$$L_m \frac{di_m}{dt} = v_2 \rightarrow i_m(t) = -I_m^{min} + \frac{v_2}{L_m}(t-t_3) , \tag{8}$$

$$L_k \frac{di_k}{dt} = v_k - nv_2 \rightarrow i_k(t) = -I_k^{min} + \frac{v_k - nv_2}{L_k}(t-t_3) . \tag{9}$$

Considering the operating intervals of the converter, two points should be taken into account. First, as shown in Fig. 3, at any moment, regardless of dead times, only one switch is turned off. This situation is similar to a synchronous boost structure in which the switches operate complementarily to enable the converter to become bidirectional.

Consequently, the proposed converter provides a bidirectional path for power flow between different ports. For example, S_1 and S_2 operate as the complements of S_3. Moreover, a similar operation exists among S_2, S_1, and S_3.

Second, according to operating intervals, the soft-switching condition for switches S_2 and S_3 can be achieved by current i_k. That is, although currents i_1 and i_2 depend on the power flow direction, current i_k is completely in accordant with the soft-switching operation of these switches. Therefore, by selecting the proper value for L_k and C_k, soft switching can be achieved for any power flow direction mode. In spite of this, the soft-switching operation of switch S_1 only depends on switch S_1. Consequently, it is turned on in a ZVS condition only if port 1 supplies the other ports. The soft-switching operation of the switches is discussed in the next sections.

IV. DESIGN CONSIDERATION

In this section, different aspects of the converter design are investigated. The most important considerations that should be taken into account in designing the converter are the voltage gain of the converter, voltage and current stresses of the semiconductor components, criteria to achieve ripple-free current for port 2, and soft-switching condition.

A. Voltage Gain Derivation

The capacitor voltages can be derived based on the voltage balance of the magnetic components. According to the voltage balance law, the integration of the voltages across L_1, L_m, and L_k should be zero. Consequently, the following relations can be derived:

$$V_k = V_2 , \tag{10}$$

$$V_o = \frac{V_1}{1-D_1} , \qquad V_o = \frac{V_2}{1-D_2} , \tag{11}$$

where D_1 is the duty cycle of S_3 and D_2 is the duty cycle of S_2.

B. Ripple-free Current Criteria

To achieve the criteria of a ripple-free input current, the slope of i_2 should be equal to zero. At any moment, current i_2 is equal to $i_m(t) - n i_k(t)$. Hence, for intervals 2, 4, and 6, the input current of port 2 can be derived as follows:

$$i_2(t) = I_m^{max} - n I_k^{max} + \left[\frac{-v_o + v_2}{L_m} + n \frac{v_k - v_o - n(v_2 - v_o)}{L_k} \right](t - t_1) , \tag{12}$$

$$i_2(t) = I_m^{min} - n I_k^{min} + \left[\frac{v_2}{L_m} - n \frac{v_k - n v_2}{L_k} \right](t - t_2) . \tag{13}$$

By equalizing the slope of the abovementioned equations to zero, the criteria for achieving the ripple-free current of port 2 are derived as follows:

$$L_k = n(1 - n) L_m . \tag{14}$$

According to (14), n should be a value lower than unity.

C. Current Stress of the Switches

1) Current Stress of Switch S_1:
Considering the key waveforms of the converter (Fig. 3),

the minimum current flowing through switch S_1 can be derived as follows:

$$I_{S_1}^{min} = -I_1 - \frac{V_1 D_1 T_s}{2 L_1} . \tag{15}$$

Moreover, at the end of interval 1, in which switch S_1 is turned off, the maximum flowing current be calculated as follows:

$$I_{S_1}^{max} = I_k^{max} - I_2 . \tag{16}$$

2) Current Stress of Switch S_2
To calculate the current stress of switch S_2, i_{S2} should be calculated at times $t = t_3$ and $t = t_0$. Thus, the current stress of this switch can be derived.

$$I_{S_2}^{min} = I_2 - I_k^{max} \tag{17}$$

$$I_{S_2}^{max} = I_2 - I_1 + \frac{V_1 D_1 T_s}{2 L_1} + \frac{V_2 D_2 T_s}{2 n L_m} \tag{18}$$

3) Current Stress of Switch S_3
A similar procedure can be used to achieve the current stress of switch S_3.

$$I_{S_3}^{min} = I_1 - I_2 - I_k^{max} - \frac{V_1 D_1 T_s}{2 L_1} \tag{19}$$

$$I_{S_3}^{max} = I_1 + \frac{V_1 D_1 T_s}{2 L_1} \tag{20}$$

4) Derivation of I_k^{max}

The value I_k^{max} is the key point to derive the soft switching of the switches based on the currents' equations.

To calculate this value, when port 2 has a ripple-free current, the current ripple of L_m should be equal to the reflected ripple of i_k to the primary side of the coupled inductor. Hence, the value can be derived as follows:

$$I_k^{max} = \frac{V_2 D_2 T_s}{2 n L_m} . \tag{21}$$

D. Soft-Switching Condition

The drain-source capacitor of power MOSFETs can generate electromagnetic interface EMI noises at the switching moments. That is, in the turn-on process of a power MOSFET, the stored energy in the C_{DS} releases into the MOSFET and generates a high-frequency electromagnetic field, which results in the EMI issue. To overcome this problem, soft-switching technology is used in which C_{DS} is discharged before the switch is turned on. The soft switching exists for a switch when the current of magnetic components is able to charge a drain-source capacitor and discharges the other one in the circuit. Consequently, to achieve soft switching, the following condition should be satisfied:

1) Switch S_1:

$$I_1 > \left(\frac{C V_o}{T_{DT}} - \frac{V_1 D_1 T_s}{2 L_1} \right) . \tag{22}$$
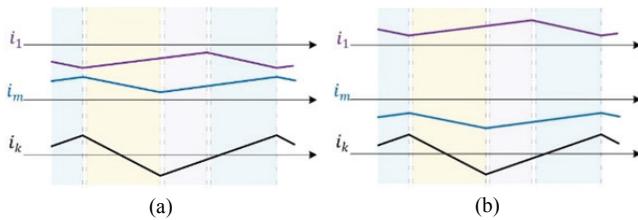
Fig. 5. Soft switching of the converter: (a) Worst-case analysis for switch S_2, (b) Worst-case analysis for switch S_3.

2) Switch S_2:

As shown in Fig. 5(a), the worst case for the soft switching of switch S_2 occurs when port 2 supplies and port 1 consumes the power. Hence, the following inequality can be derived:

$$\frac{D_2 V_2 T_S}{2nL_m} > \left(\frac{CV_O}{T_{DT}} + I_2\right). \tag{23}$$

3) Switch S_3:

As shown in Fig. 5(b), the worst case for the soft switching of switch S_3 occurs when port 1 supplies and port 2 consumes power. Therefore, the soft-switching criteria for this switch results in the following inequality:

$$\frac{D_2 V_2 T_S}{2nL_m} > \left(\frac{CV_O}{T_{DT}} + \frac{V_1 D_1 T_S}{2L_1} + I_2 - I_1\right). \tag{24}$$

According to (20), the soft-switching condition for switch S_1 only satisfies when port 1 supplies power to other ports. Moreover, based on (21) and (22), to achieve soft-switching condition for switches S_2 and S_3, the value of nL_m should be lower than a specific value. Consequently, the coupled inductor should be designed based on (14), (23), and (24).

V. EXPERIMENTAL RESULTS

The operating modes of the converter generally involve ports 1 and 2 supplying the output, port 1 supplying port 2 and the output, and so on; thus, the current waveforms of the switches vary. In this section, the operations of the converter are validated in different operating modes by using the experimental results. Three operating modes of the converter were examined in the laboratory to validate the performance of the converter containing the soft-switching operation of the converter, bidirectional power flow capability, and ripple-free input current of port 2.

The parameters of the prototype are presented in Table I. As shown in the table, to achieve soft switching of the switches, (23) and (24) are used. Based on this equations, the value of nL_m was set to 12 μ. By selecting a small value for n, the secondary side of the coupled inductor experiences high current [21]. Therefore, the turn ratio and magnetizing inductance were selected as $n=0.25$ and $l_m=48 \ μH$. In addition, for ripple-free current of port 2, a leakage inductance of $8.5 \ μH$ is required using (14). Although a special winding approach was proposed in Ref. [21] to actuate a leakage inductor, an

TABLE I
CHARACTERISTICS OF THE EXPERIMENTAL PROTOTYPE

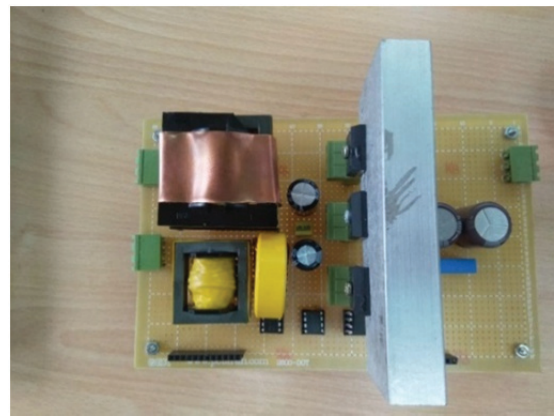| Parameter	Value
V_1: Voltage source of port 1	35 V
V_2: Voltage source of port 2	48 V
V_o: Output voltage across the load	100 V
P_O: Rated power	200 W
L_1: Inductor of port 1	100 μH
L_m: Magnetizing inductance of coupled inductor	48 μH
L_k: Leakage inductance of coupled inductor	8.5 μH
n: Coupled inductor turn ratio	0.25
C_k: Balancing capacitor	4.7 μF
C: Output capacitor	100 μF

Fig. 6. Experimental prototype of the proposed converter.

external *7 μH* inductor was added in series with the secondary side of the inductor to achieve a ripple-free feature in this study. To select the core size of the coupled inductor, the core geometry approach (K_g) was used. The design was conducted similarly with a flyback transformer based on the step-by-step method proposed in Ref. [22].

According to this approach, the calculated core geometry is equal to K_g=0.09, which approximates that of ETD29 ferrite core. A similar procedure was conducted to design the core size of inductor L_1, which leads to a ETD34 ferrite core. An image of the prototype is shown in Fig. 6.

The control and modulation system is shown in Fig. 7. As shown in the figure, the status of the converter, including currents and voltages, is sensed. The signals are sent to microcontroller STM32F407VGT6. In the microcontroller, the compensators and mode selection system similar to Ref. [15] can be used to determine duty cycles D_1 and D_2. However, as this study aims to show bidirectional operation and soft switching of the converter, a simple control approach was used.

In this study, two PI compensators were used to control the output voltage and input current i_1. The current control loop tunes duty cycle D_1 and the voltage control loop determines D_2. To provide gate pulses, a CPLD-xc9572 was used, in
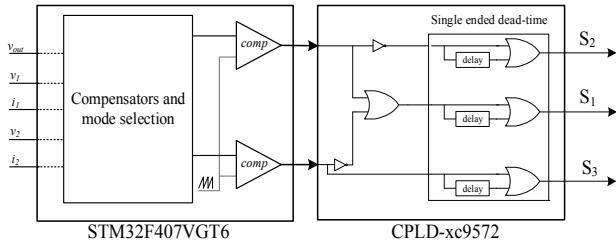
Fig. 7. Control diagram of the proposed converter.

TABLE II
PERFORMANCE COMPARISON

Parameters	Ref. [6]	Ref. [19]	Proposed converter
No. of switches	3	4	3
No. of diodes	0	2	0
Magnetic components	2	2	2
No. of capacitors	1	1	2
Bidirectional operation	No	Yes	Yes
Soft switching	No	No	Yes
Input ripple	Low ripple	High ripple	Low ripple-Ripple free
Voltage gain	$\dfrac{1}{1-D}$	$\dfrac{D_i}{1-D}$	$\dfrac{1}{1-D}$
Single mode	Yes	Yes	Yes

which a combinational–sequential structure was implemented. In the first scenario, the operation of the converter when ports 1 and 2 supply the output is considered. Accordingly, i_1 and i_2 are greater than zero and the bottleneck for the soft-switching condition is switch S_2. Fig. 8 illustrates the experimental results. For clarity, intervals 2, 4, and 6 are highlighted in the figure. As previously mentioned, in interval 2, switches S_1 and S_3 are turned on. Therefore, i_2 flows through switch S_1 in the opposite direction to supply the load. However, current i_k, which flows through S_1, starts from a positive value and ends with a negative value. Therefore, at the end of this interval, the current of switch S_1 obtains a positive value, which validates the soft-switching operation of switch S_2 in the next interval [Fig. 8(a)]. Similarly, in interval 4 in which switches S_2 and S_3 are turned on, both input currents store energy into the input inductors. During this interval, i_k starts from a negative value and ends with a positive value. At the end of this interval, as $i_1>0$, switch S_1 becomes ready for soft switching in the next interval [Fig. 8(b)].

Interval 6 starts with the soft switching of switch S_1. In this interval, i_k increases, and at the end of the interval, it reaches to the maximum value. Consequently, $i_k-i_1+i_2>0$ and S_3 is turned on in a soft-switching condition. Moreover, the ripple-free current of port 2 is validated in Fig. 8d. As shown in the figure, the magnetizing inductance of the coupled inductor is a half of the inductor of port 1, and the ripple of port 2 is lower than that of port 1.

Similarly, soft switching exists for the two other modes (Figs. 9 and 10). As shown in Fig. 9, port 2 supports two

other ports. In this mode, which is shown in Fig. 9, i_2 is positive and i_1 is negative. Accordingly, the bottleneck for the soft switching of the converter is switch S_2. The soft switching of switches S_1, S_2, and S_3 are illustrated in Figs. 9a–9d. In particular, the figures show the main intervals 2, 4, and 6. In Fig. 8, the same finding can be considered for this mode.

The last scenario is a situation in which port 1 supplies power to the other ports (Fig. 10). In this case, switch S_3 may fail to operate in a soft-switching condition. However, by selecting the appropriate values for turn ratio and magnetizing the inductance of the coupled inductor, the experimental results validate the operation of this switch in the soft-switching condition.

To increase the clarity of the soft-switching operation of the proposed converter, the gate-source and drain-source voltages of the switches are shown in Fig. 11. As shown in the figure, all switches operate in a zero-voltage condition, as the drain-source voltage reaches zero before the gate-source pulse is applied to the switch. In addition, to validate the operation of the converter in transitions between two steady-state conditions, the dynamic performance of the converter is illustrated in Fig. 12. The figure presents the performance of the converter for a 100 W output load, in which port 1 first supports the output load. However, after a special instant, port 1 consumes power and port 2 supplies the output load.

To illustrate the advantages of the proposed converter with respect to the newly proposed converter, a comparison was conducted between the proposed converter and two other multiport converters. As shown in Table II, through the coupled inductor, the proposed converter operates in a soft-switching condition. Moreover, the improved switching strategy leads to the bidirectional operation with respect to Ref. [6]. In comparison to Ref. [6], the converter has the advantages of soft switching and bidirectional operation. Then, in comparison to Ref. [19], the soft switching, few utilized components, and high voltage gain are the most important benefits. In accordance with the converter proposed in Ref. [6], the voltage stress of the switches in both converters is the same. However, to achieve a ripple-free current for port 2, current i_k results in an extra current stress on the switches. Therefore, the current stress of the switches increases by a value of $(1-n)I_k^{max}$.

The efficiency of the converter is discussed in this section. The efficiency of the converter relates to the losses of the converter. The losses of the proposed converter mainly include two important parts:

- Magnetic component losses
- Switch losses

The magnetic losses contain the conduction losses of the windings and core losses.

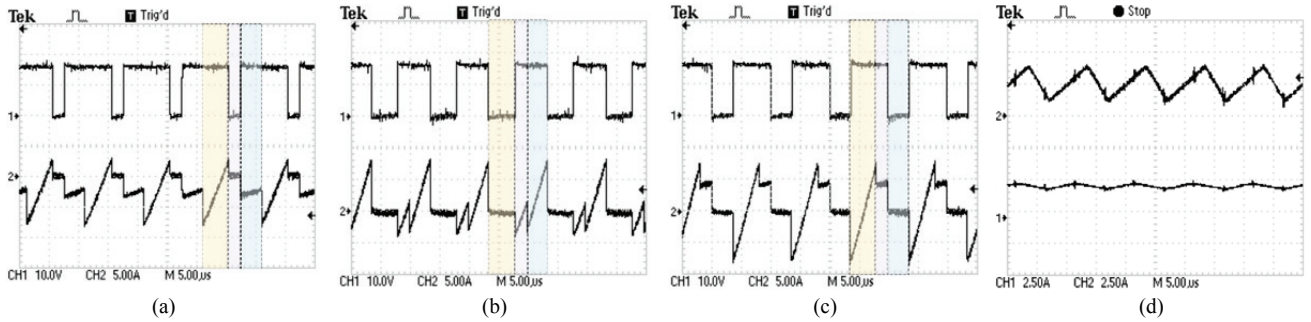$$P_{mag} = P_{mag,core} + P_{mag,con} = \sum_W R_w I_{W,rms}^2 + P_{mag,core}. \tag{23}$$

Fig. 8. Soft-switching operation of the switches when V_1 and V_2 support the output load: (a) CH1: V_{GS} and CH2: i_D of switch S_1, (b) CH1: V_{GS} and CH2: i_D of switch S_2, (c) CH1: V_{GS} and CH2: i_D of switch S_3, (d) CH1: i_2 and CH2: i_1.
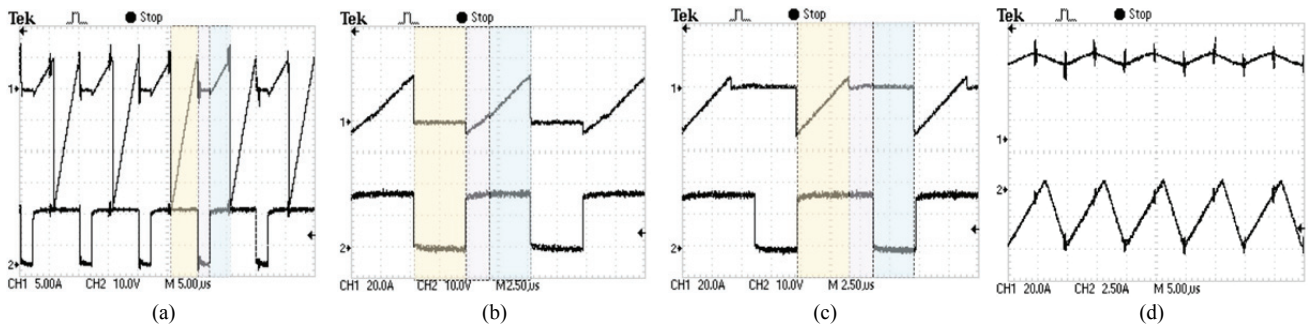

Fig. 9. Soft-switching operation of the switches when V_2 supports the output load and V_1 : (a) CH2: V_{GS} and CH1: i_D of switch S_1, (b) CH2: V_{GS} and CH1: i_D of switch S_2, (c) CH2: V_{GS} and CH1: i_D of switch S_3, (d) CH1: i_2 and CH2: i_1.
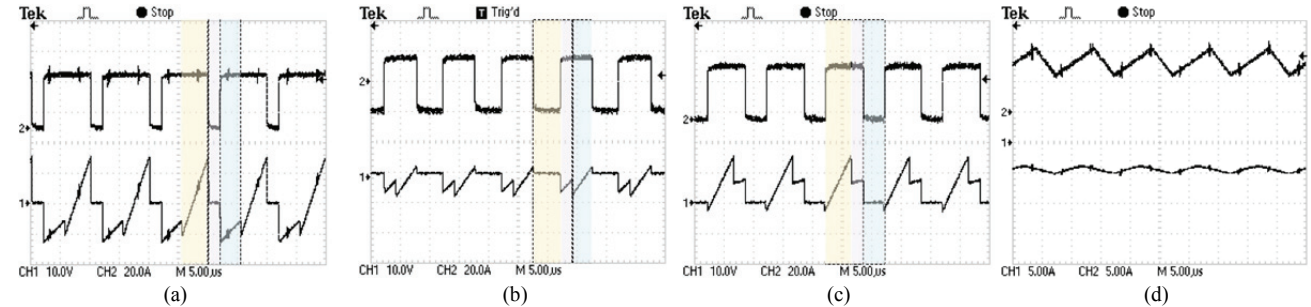

Fig. 10. Soft-switching operation of the switches when V_1 supports V_2 and the output load: (a) CH2: V_{GS} and CH1: i_D of switch S_1, (b) CH2: V_{GS} and CH1: i_D of switch S_2, (c) CH2: V_{GS} and CH1: i_D of switch S_3, (d) CH1: i_2 and CH2: i_1.
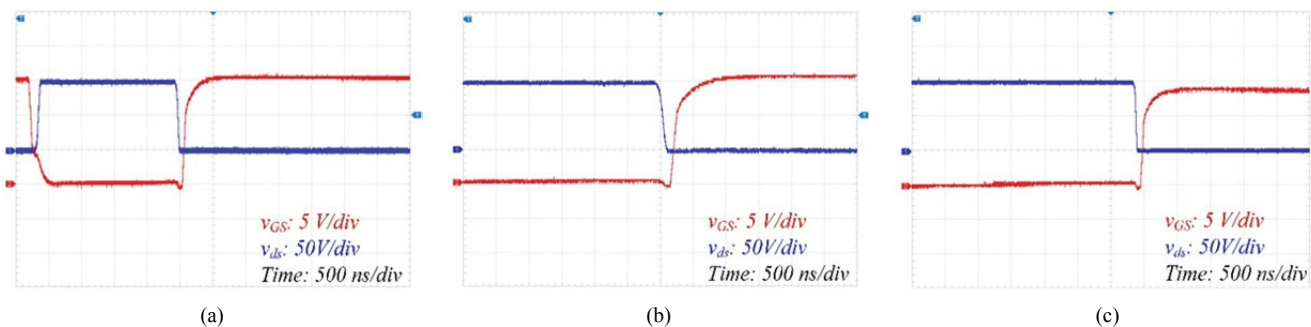

Fig. 11. Soft-switching validation of the switches of the proposed converter. Drain-source voltage versus gate-source voltage related to: (a) Switch 1, (b) Switch 2, (c) Switch 3.

Moreover, the switch losses include switching and conduction losses. The switching losses can be calculated based on the voltage and current waveforms as follows:

$$P_{switching} = \frac{1}{2} f_s V_{DS} I_D t_{off} , \qquad (24)$$

1301

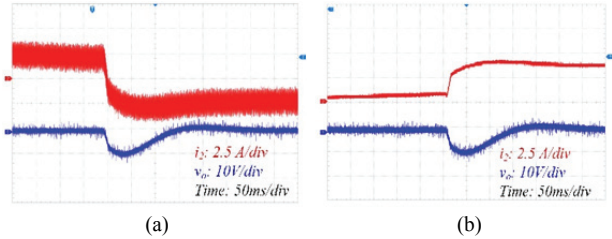(a)   (b)

Fig. 12. Dynamic performance of the converter parameters: (a) Output voltage versus port 1 current, (b) Output voltage versus port 2 current.
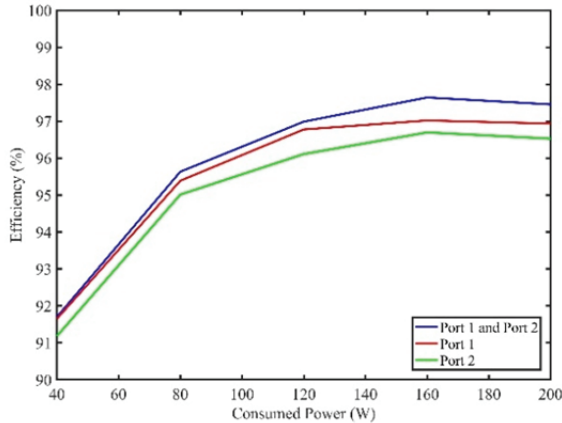

Fig. 13. Efficiency of the converter for different operating modes.

where t_{off} is the turn-off transition of the switches. Moreover, the conduction losses of the converter can be calculated as follows:

$$P_{conduction} = \sum_w R_{S_i} I_{S_i,rms}^2 . \tag{25}$$

Considering the selected switch for the prototype, which is FDP2532, the efficiency of the prototype for different operation modes is illustrated in Fig. 13. The figure shows the efficiency of the converter for three different conditions. The first condition is when the output port is supplied by two ports (blue line), the second condition is when port 1 supplies the other ports (red line), and the third condition is when port 2 provides the required power of the other ports (green line).

VI. CONCLUSION

Bidirectional multi-input DC–DC converters are interesting structures for hybrid supply systems. In this study, a three-port soft-switching DC–DC converter was proposed. A coupled inductor was utilized and a modified switching strategy was proposed. Subsequently, the converter provided a ripple-free current port, and bidirectional operation between each port was achieved. In addition, the soft-switching operation of the converter, in which the entire set of switches operate in a soft-switching condition, was realized. The soft-switching operation loses in one operating mode for one switch. Thus, the converter should be utilized for renewable energy resource applications. In particular, the renewable

source should be connected to port 1 to enable the converter to continuously operate in soft-switching conditions.

REFERENCES

[1] H. Moradisizkoohi, J. Milimonfared, M. Taheri, and S. Salehi, "A high step-up half-bridge DC/DC converter with a special coupled inductor for input current ripple cancelation and extended voltage doubler circuit for power conditioning of fuel cell systems," *Int. J. Circuit Theory Appl,*Vol. 44, No. 6, pp. 1290-1307, Jun. 2016.

[2] S. A. Arshadi, B. Poorali, E. Adib, and H. Farzanehfard, "High step-up DC-AC inverter suitable for AC module applications," *IEEE Trans. Ind. Electron.*, Vol. 63, No. 2, pp. 832-839, Feb. 2016.

[3] W. Liang, Y. Liu, B. Ge, and H. Abu-Rub, "Investigation on pulse width amplitude modulation based single-phase quasi-z-source photovoltaic inverter," *IET Power Electron.* Vol. 10, No.14, pp. 832-839, Nov. 2017.

[4] B. Gu, J. Dominic, J. S. Lai, Z. Zhao, and C. Liu, "High boost ratio hybrid transformer DC-DC Converter for photovoltaic module applications," *IEEE Trans. Power Electron.*, Vol. 28, No. 4, pp. 2048-2058, Jun. 2013.

[5] J. Wei and B. Fahimi, "Maximum solar power transfer in Multi-port Power Electronic Interface," in *Applied Power Electronics Conference and Exposition (APEC), IEEE*, pp. 68-73, 2010.

[6] M. Mohammadi, J. Milimonfared, M. R. M. Behbahani, J. S. Moghani, and H. Moradi, "A double-input DC-DC converter for hybrid supply systems," in *6th Annual International Power Electronics, Drive Systems, and Technologies Conference, (PEDSTC)* , pp. 29-34, 2015.

[7] M. Delshad, A. T. Harchegani, M. Karimi, and M. Mahdavi, "A new ZVT multi input converter for hybrid sources systems," in *International Conference on Applied Electronics (AE)* , pp. 61-64, 2016.

[8] S. Xiaofeng, P. Guangming, Y. Shuai, and C. Zhe, "A novel multi-port dc/dc converter with bi-directional storage unit," in *Power Electronics and Motion Control Conference (IPEMC),* pp. 1771-1775, 2012.

[9] Y. Chen, A. Huang, and X. Yu, "A High Step-Up Three-Port DC-DC Converter for Stand-Alone PV/Battery Power Systems," *IEEE Trans. Power Electron.*, Vol. 28, No. 11, pp. 5049-5062, Nov. 2013.

[10] A. Lahyani, P. Venet, A. Guermazi, and A. Troudi, "Battery/supercapacitors combination in uninterruptible power supply (UPS)," *IEEE Trans. Power Electron.*, Vol. 28, No. 4, pp. 1509-1522, Jul. 2013.

[11] A. Khaligh, C. Jian, and L. Young-Joo, "A multiple-input DC-DC converter topology," *IEEE Trans. Power Electron.*, Vol. 24, No. 3, pp. 862-868, Jan. 2009.

[12] H. Matsuo, T. Shigemizu, F. Kurokawa, and N. Watanabe, "Characteristics of the multiple-input DC-DC converter," in *Power Electronics Specialists Conference,. (PESC), IEEE*, pp. 115-120, 1993.

[13] H. Matsuo, L. Wenzhong, F. Kurokawa, T. Shigemizu, and N. Watanabe, "Characteristics of the multiple-input DC-DC converter," *IEEE Trans. Ind. Electron.*, Vol. 51, No. 3, pp. 625-631, Jun. 2004.

[14] Z. Qian, O. Abdel-Rahman, and I. Batarseh, "An integrated

four-port DC/DC converter for renewable energy applications," *IEEE Trans. Power Electron.*, Vol. 25, No. 7, pp. 1877-1887, Jul. 2010.

[15] W. Hongfei, S. Kai, D. Shun, and X. Yan, "Topology derivation of nonisolated three-port DC-DC converters from DIC and DOC," *IEEE Trans. Power Electron.*, Vol. 28, No. 7, pp. 3297-3307, Oct. 2013.

[16] R. Jie, L. Fuxin, R. Xinbo, Y. Dongsheng, L. Yan, and J. Ke, "Isolated multiple-input DC/DC converter using alternative pulsating source as building cells," in *International Power Electronics Conference (IPEC),* pp. 1463-1470, 2010.

[17] Z. Qian, "Modeling and Design of Multi-port Dc/dc Converters," PhD. Thesis, UCF Florida 2010.

[18] B. Mangu, S. Akshatha, D. Suryanarayana, and B. G. Fernandes, "Grid-connected PV-wind-battery-based multi-input transformer-coupled bidirectional DC-DC converter for household applications," *IEEE J. Emerg. Sel. Top. Power Electron.*, Vol. 4, No. 3, pp. 1086-1095, Sep. 2016.F.

[19] F. Akar, Y. Tavlasoglu, E. Ugur, B. Vural, and I. Aksoy, "A bidirectional nonisolated multi-input DC-DC converter for hybrid energy storage systems in electric vehicles," *IEEE Trans. Veh. Technol*, Vol. 65, No. 10, pp. 7944-7955, Oct. 2016.

[20] P. Zhang, Y. Chen, and Y. Kang, "Nonisolated wide operation range three-port converters with variable structures," *IEEE J. Emerg. Sel. Top. Power Electron.*, Vol. 5, No. 2, pp. 854-869, Jun. 2017.

[21] D. Hyun-Lark, "Improved ZVS DC-DC converter with a high voltage gain and a ripple-free input current," *IEEE Trans. Circuits Syst. I Reg. Papers*, Vol. 59, No. 4, pp. 846-853, 2012.

[22] C. W. Mclyman, *Transformer and Inductor Design Handbook*. CRC Press, Nov. 2004.

Parastou KhademiAstaneh was born in Ardabil, Iran. She received her B.S. and M.S. in Electrical Engineering from Iran University of Science and Technology, Tehran, Iran, in 2008 and 2010, respectively. She is currently pursuing her Ph.D. degree in the University of Mohaghegh Ardabili, Ardabil, Iran. Her current research interests include power electronics and renewable energy.

Javad Javidan received his B.Sc. and M.Sc. and Ph.D. degrees in Electrical Engineering from Sharif University of Technology, Tehran, Iran, in 2001 and 2003, respectively. He also received his Ph.D. degree from Sharif University of Technology in the field of RFIC design in 2010. He received a one-year grant from Hong Kong University of Science and Technology for doing his research as a RA and visiting student. He is currently an Assistant Professor at the University of Mohaghegh Ardabili, Ardabil, Iran. His main research interests are power electronics and renewable energy, F/analog/mixed-signal ICs, and integrated circuits for digital receivers.

Khalil Valipour was born in Ardabil, Iran. He received his B.S., M.S., and Ph.D. degrees in Electrical Engineering. Currently, he is an Assistant Professor at the Department of Technical Engineering, University of Mohaghegh Ardabili, Ardabil, Iran. His research interests are power system dynamics, power system modeling in transient states, electrical machine and transformer design, reactive power control, protective relays, and renewable energy management.

Adel Akbarimajd received his B.Sc. degree in Control Engineering from Ferdowsi University of Mashhad, Mashhad, Iran, in 1997 and M.Sc. degree in Control Systems from Tabriz University of Iran, Tabriz, Iran, in 2000. He received his Ph.D. degree in AI and Robotics from the University of Tehran, Tehran, Iran, in 2009. In 2007, he spent six months in the Biorobotics Laboratory, EPFL, Lausanne, Switzerland, as a visiting researcher. Later, he moved to the Department of Engineering, University of Mohaghegh Ardabili, Ardabil, Iran, where he is currently an Associate Professor. He was the Head of the Department of Electrical and Computer Engineering, University of Mohaghegh Ardabili, from 2011 to 2016. His research interests include planning and control of power systems and robotic systems.